Optimization of optically-driven micromachines

Vincent L. Y. Loke, Theodore Asavei, Timo A. Nieminen,
Norman R. Heckenberg and Halina Rubinsztein-Dunlop

School of Mathematics and Physics, The University of Queensland,
Brisbane QLD 4072, Australia

ABSTRACT

While a variety of different optically-driven micromachines have been demonstrated by a number of groups around the world, there is a striking similarity in the designs used. The typical optically-driven rotor consists of a number of arms attached to a central hub, or elongated stalk in the case of free-floating rotors. This is a consequence of the relationship between the symmetry of a scattering object and the transfer of optical angular momentum from a beam to the object.

We use a hybrid discrete-dipole approximation/T-matrix method algorithm to computationally model the scattering by such optically-driven rotors. We systematically explore the effects of the most important parameters of rotors, such as the thickness, length, and width of the arms, in order to maximize the torque efficiency.

We show that it is possible to use computational modelling to optimize the design of such devices. We also compare the computational results with experiment.

Keywords: micromachines, microrotors, DDA, T-matrix, symmetry optimization

1. INTRODUCTION

1.1 Optical tweezers

Microscopic particles can be trapped via the 'gradient force' using a tightly focussed Gaussian laser beam. This single-beam trapping was first demonstrated at AT&T Bell Laboratories[1] in 1985. This type of optical trap is commonly called *optical tweezers*, and is based upon transfer of linear momentum of light by scattering. Optical tweezers can also apply torque based on the transfer of angular momentum, either orbital or spin angular momentum. Spin angular momentum is carried by a beam with circular or elliptical polarization whereas, for example, a Laguerre–Gauss (LG) beam carries orbital angular momentum about the beam axis.

Both spin[2] and orbital[3] angular momenta can be transferred through absorption; the resulting heating makes this method impractical for most purposes. Alternatively, if the particle changes the angular momentum of the incident beam, there will an angular momentum transfer which results in torque on the particle. Spin angular momentum can be transferred to particles with either microscopic material birefringence[4,5] or form birefringence.[6] Orbital angular momentum can be transferred by making use of non-axisymmetric beams[7] on microrotors.[8] In this paper we model the torque on specially designed and fabricated micro objects when trapped and rotated using LG_{0l} beams, where l is the azimuthal mode index.

Further author information: (Send correspondence to V.L.Y.L.)
V.L.Y.L.: E-mail: loke@physics.uq.edu.au, Telephone: 61 7 33653405

Optical Trapping and Optical Micromanipulation VI, edited by Kishan Dholakia, Gabriel C. Spalding, Proc. of SPIE
Vol. 7400, 74001Z · © 2009 SPIE · CCC code: 0277-786X/09/$18 · doi: 10.1117/12.828423

1.2 The microrotor

Microrotors are likely to be key components for micromachines in microengineering or microfluidic applications. As part of the design process we employ computational methods to optimize the structure of the microrotor for optimal torque efficiency. We fabricate microrotors using two-photon photopolymerization[9] and they are usually driven using LG_{02} or LG_{04} beams. The method we use to determine torque efficiency experimentally[10,11] involves measuring the rate of rotation and the change in circular polarization.

We propose a basic design of a quatrefoil rotor (figure 1) which is is fan shaped, axle mounted with caps on the ends of the axle to restrict movement along the beam axis; its size will be in the order of a few microns. The actual dimensions of the prototype, i.e., blade radius, hub radius, height and blade angle, will be based on the computer simulated results for optimal torque. The quatrefoil rotor will operate in water where the wavelength of the incident beam will be 798 nm.

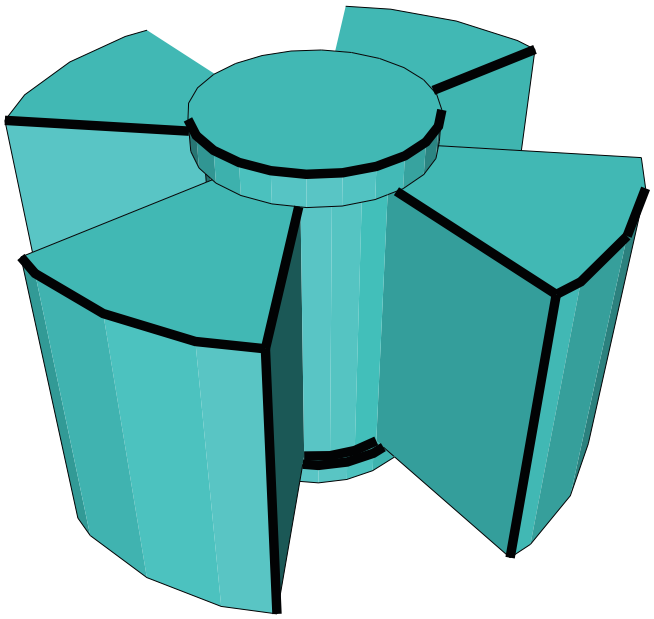

Figure 1. Quatrefoil axle mounted microrotor.

2. COMPUTATIONAL MODELLING

2.1 Modelling methods

Equipped with the combination of the methodologies below, it is possible to model a complex mesoscopic structure that is several microns in size. Without symmetry optimizations, the memory requirements would exceed that available on a high-end desktop PC. Moreover, the time taken to calculate the T-matrix for a single microrotor would be in the order of weeks. To optimize the design of a microrotor, we need to alter its dimensions; this involves calculating well over a hundred T-matrices.

The calculations are performed using MATLAB on a high-end desktop PC. Some of the functions used were from the Optical Tweezers Toolbox[12] library.

2.2 VSWFs and *T*-matrix

Electric fields (and similarly for magnetic fields) can be represented as multipole expansions of incident and scattered vector spherical wave functions (VSWFs)

$$\mathbf{E}_{\text{inc}} = \sum_{n=1}^{N_{max}} \sum_{m=-n}^{n} a_{nm}\mathbf{M}_{nm}^{(3)} + b_{nm}\mathbf{N}_{nm}^{(3)}, \tag{1}$$

$$\mathbf{E}_{\text{scat}} = \sum_{n=1}^{N_{max}} \sum_{m=-n}^{n} p_{nm}\mathbf{M}_{nm}^{(1)} + q_{nm}\mathbf{N}_{nm}^{(1)}. \tag{2}$$

where a_{nm} and b_{nm} are the incident coefficients, p_{nm} and q_{nm} are the scattering coefficients, n is the radial mode index, m is the azimuthal mode index and $\mathbf{M}$ and $\mathbf{N}$, orthonormal eigenfunctions of the vector Helmholtz equation, are known as vector spherical wave functions (VSWFs).[13] The number of terms are truncated to N_{max}, determined by a radially-based criterion.[14]

T-matrix connects the coefficients of the scattered and incident fields. The T-matrix characterizes the light scattering properties of a particle for a given wavelength

$$\begin{bmatrix} p_{nm} \\ q_{nm} \end{bmatrix} = \mathbf{T} \begin{bmatrix} a_{nm} \\ b_{nm} \end{bmatrix}. \tag{3}$$

The main advantage of the T-matrix is that it only has to be calculated once fro a given object. If the illumination changes, incident beam coefficients can be quickly calculated and the above operation by the T-matrix (3) takes merely seconds.

2.3 DDA

The discrete dipole approximation[15,16] (DDA), sometimes referred to as the coupled-dipole method (CDM), is a method of modelling scattering by particles with arbitrary shapes and allows for inhomogeneous and anisotropic materials. This method can be applied to objects ranging from Rayleigh particles to large particles (of size many times the wavelength); the size is limited by computational time and available RAM.

The particle/scatterer is represented by point dipoles (figure 2) numbered $j = 1, ..., N$ with polarizabilities α_j located at positions r_j; we do not anticipate that the axle caps (in figure 1) will have much effect on the incident beams and thus they are not included in the model. Each dipole has polarization

$$\mathbf{P}_j = \alpha_j \mathbf{E}_j, \tag{4}$$

where α_j is the polarizability tensor[16] and $\mathbf{E}_j$ is the time harmonic $\mathbf{E}$-field amplitude at each dipole location r_j due to the incident field $\mathbf{E}_{inc,j} = \mathbf{E}_0 \exp(\mathrm{i}kr_j\mathrm{i}\omega t)$ plus contributions from $N-1$ dipoles:

$$\mathbf{E}_j = \mathbf{E}_{inc,j} - \sum_{k \neq j} \mathbf{A}_{jk}\mathbf{P}_j, \tag{5}$$

where the off-diagonal 3×3 tensors of the interaction matrix are

$$\mathbf{A}_{jk} = \frac{\exp(\mathrm{i}kr_{jk})}{r_{jk}} \left[k^2(\hat{r}_{jk}\hat{r}_{jk} - \mathbf{1}_3) + \frac{\mathrm{i}kr_{jk} - 1}{r_{jk}^2}(3\hat{r}_{jk}\hat{r}_{jk} - I_3) \right], \; j \neq k, \tag{6}$$

where r_{jk} is the distance from points r_j to r_k, $\hat{r}_{jk}$ is the unit vector in the direction from points r_j to r_k. Defining the diagonal tensors as $\mathbf{A}_{jj} = \alpha_j^{-1}$, and substituting into equations 4 and 5,

$$\mathbf{E}_{inc,j} = \mathbf{A}_{jj}\mathbf{P}_j + \sum_{k \neq j} \mathbf{A}_{jk}\mathbf{P}_j, \tag{7}$$

the problem is reduced to solving $3N$ unknown polarizations $\mathbf{P}_j$ in the following system of $3N$ linear equations:

$$\sum_{k=1}^{N} \mathbf{A}_{jk}\mathbf{P}_j = \mathbf{E}_{inc,j}. \tag{8}$$

$\mathbf{A}_{jk}$ is a square matrix. Once $\mathbf{P}_j$ is known, the field, force, torque and other quantities of interest can be calculated.

2.4 Near field point-matching

The near field calculated via DDA can be matched to scattered field (2) expressed in terms of VSWFs at points around the scatterer (figure 3). Since we have the dipole moments, P_j, we can derive a 'field matrix', $\mathbf{F}_{ij}$, derived from equations of electric dipole fields[17] such that

$$\mathbf{E}_i^{(DDA)} = \sum_{i=1}^{N_{PM}} \mathbf{F}_{ij}\mathbf{P}_j, \tag{9}$$

where N_{PM} is the number of points to be matched, j is the index for the dipole, i is the index for the near field point and field matrix, $\mathbf{F}_{ij}$, is made up of 3×3 tensors

$$\mathbf{F}_{ij} = \frac{\exp(\mathrm{i}kr_{jk})}{r_{jk}} \left[k^2(\hat{r}_{jk}\hat{r}_{jk} - \mathbf{1}_3) + \frac{\mathrm{i}kr_{jk} - 1}{r_{jk}}(3\hat{r}_{jk}\hat{r}_{jk} - \mathbf{1}_3) \right], \tag{10}$$

where $\hat{r}_{jk}$ is the unit vector between a dipole and a matched point.

Rotational and mirror symmetry optimizations[18] may also be applied to (9) such that we only need to calculate the fields of the matched points in one octant:

$$\mathbf{E}_i^{(DDA,oct)} = \sum_{i=1}^{N_{PM}/8} \mathbf{F}_{ij}^{(oct)}\mathbf{P}_j^{(oct)}, \tag{11}$$

where only the fields for an octant are calculated (although all the dipole moments are used). Thus reduces the number of equations by a factor of 64 compared to (9). Given the VSWF expansion of the scattered field in (2), we can solve for the scattering coefficients

$$\begin{aligned} p_{nm} &= \mathbf{M}_{nm}^{(1)}(kr)/\mathbf{E}_{TE,nm}^{(DDA)}, \\ q_{nm} &= \mathbf{N}_{nm}^{(1)}(kr)/\mathbf{E}_{TM,nm}^{(DDA)}. \end{aligned} \tag{12}$$

As we cycle through each combination of n and m, we obtain the solutions for the scattering coefficients p_{nm} and q_{nm} which represent coupling between the n and m incident and scattered modes; p_{nm} and q_{nm} together make up one column of the T-matrix at a time.

2.5 Symmetry optimizations

The symmetry optimization employed for the calculations is discussed in detail in our previous publication.[18] In addition to the scheme in (11) for the point-matching method, the discrete rotational symmetry of a scatterer can be similarly exploited, using phase relations, to reduce the memory footprint and computational time for the DDA calculations.

When calculating the T-matrix, we further exploited the discrete rotational symmetry of the scatterer using Floquet's theorem to bypass calculations for redundant scattered modes. Also, if the scatterer, in this case the quatrefoil rotor, is always on the beam's axis, and the type of illumination is always known, we only need to cycle through a limited number of incident modes.

By combining these optimization methods memory and computational time savings of at least 2 orders of magnitude can be attained.

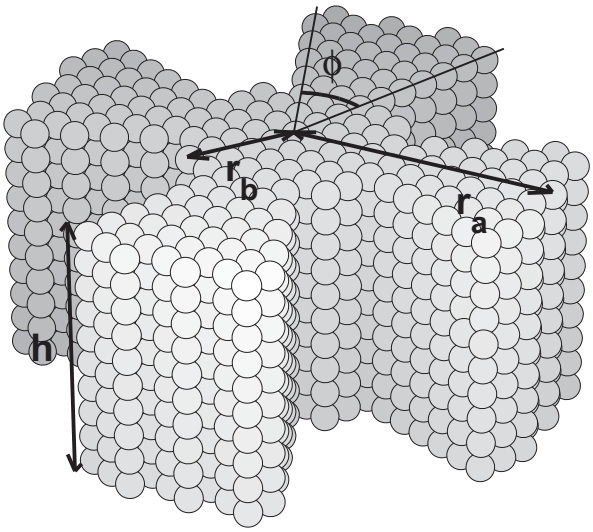

Figure 2. Dipole model of the quatrefoil microrotor.

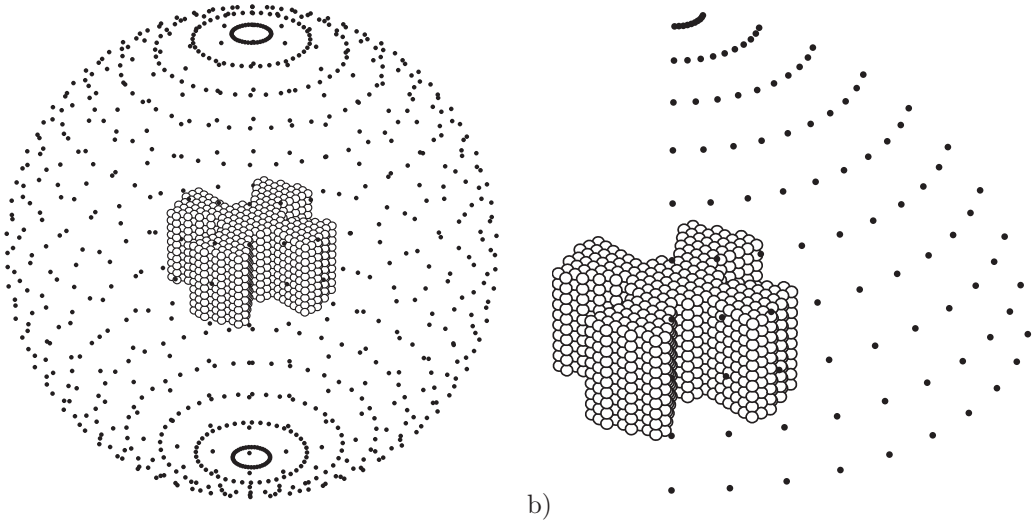

a) b)

Figure 3. a) Near field matching and b) octant near field matching for a dipole model of the quatrefoil rotor.

2.6 Torque calculation

The linear momentum and the angular momentum fluxes are calculated using the explicit evaluation of Clebsch–Gordan coefficients.[19] The momentum flux divided by the incident power gives the axial trapping efficiency:

$$\begin{aligned} Q &= \frac{2}{P_{\text{inc}}} \sum_{n=1}^{\infty} \frac{1}{n+1} \sum_{m=-n}^{n} \Big\{ \frac{m}{n} \text{Re}(a_{nm}^* b_{nm} - p_{nm}^* q_{nm}) \\ &\quad + \left[\frac{n(n+2)(n-m+1)(n+m+1)}{(2n+1)(2n+3)} \right]^{1/2} \\ &\quad \times \text{Re}(p_{nm} p_{n+1,m}^* + q_{nm} q_{n+1,m}^* - a_{nm} a_{n+1,m}^* - b_{nm} b_{n+1,m}^*) \Big\} , \end{aligned} \tag{13}$$

in units of $n\hbar k$ per photon (relating to $\hbar\omega$ energy of the wave) and P_{inc} is the power of the incident beam. The angular momentum flux divided by the incident power gives the torque efficiency (or normalized torque) about

the beam axis:

$$\tau_z = \sum_{n=1}^{N_{max}} \sum_{m=-n}^{n} m(|a_{nm}|^2 + |b_{nm}|^2 - |p_{nm}|^2 - |q_{nm}|^2)/P_{\text{inc}} \tag{14}$$

in units of $\hbar$ per photon. The incident beam power P_{inc} in units of $\hbar$ per photon is

$$P_{\text{inc}} = \sum_{n=1}^{N_{max}} \sum_{m=-n}^{n} |a_{nm}|^2 + |b_{nm}|^2. \tag{15}$$

3. RESULTS

3.1 Laguerre–Gauss trapping and driving beams

We intend to trap and rotate the fabricated microrotors with Laguerre–Gauss LG_{02} and LG_{04} beams, tightly focussed with the beam convergence at 78°. Figures 4 and 5 show the cross-sections of the free field LG_{02} and LG_{04} beams respectively, superimposed on the cross-section of the quatrefoil rotor. The $LG_{0\ell}$ beams have low intensity cores (dark spot).

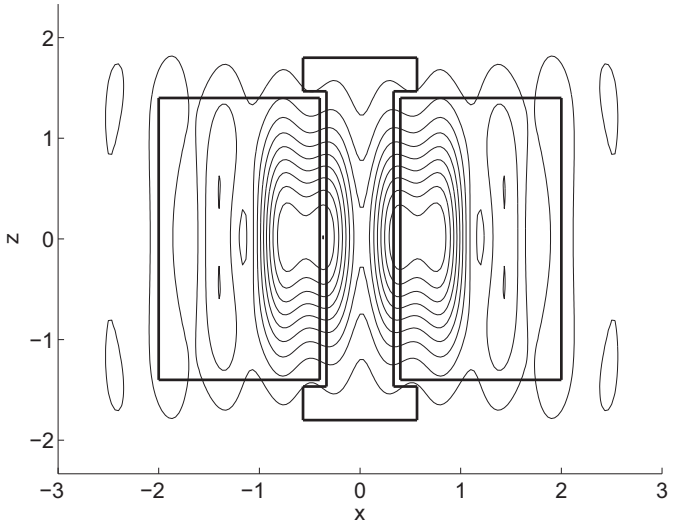

Figure 4. Intensity contour of the LG_{02} incident beam and quatrefoil rotor profile.

To model the LG incident beams we used the beam shape coefficient (BSC) far field point-matching function[20] from the Optical Tweezers Computational Toolbox[12] to obtain the incident coefficients. Applying the T-matrix to the incident beam coefficients (3), we obtained the scattering coefficients and subsequently calculated the torque using (14).

3.2 Dimensions for optimal torque

The design of micromachines is an ongoing project and our goal for the quatrefoil rotor is to find the optimal dimensions for h, r_a, r_b and ϕ. All linear dimensions are in wavelength units and the angle in radians.

First, we varied the height h whilst keeping the other dimensions constant: $\phi = \pi/4$, $r_b = 0$ and two different blade radii, $r_a = 1$ and $r_a = 2$. The torque efficiency plateaued after $h = 2.2$ for $r_a = 1$ and $h = 3.4$ for $r_a = 2$ (figure 6) which stands to reason since the beam profiles (figures 4 and 5) show a sharp drop in intensity outside that vertical region.

It is apparent thus far and in subsequent calculations that we obtain a higher torque efficiency with the LG_{02} beam. Thus, we will favour design towards the LG_{02} beam. Now keeping the rotor height at $h = 3.4$ we varied the blade radius and found the optimum at $r_a = 2.6$ (figure 7).

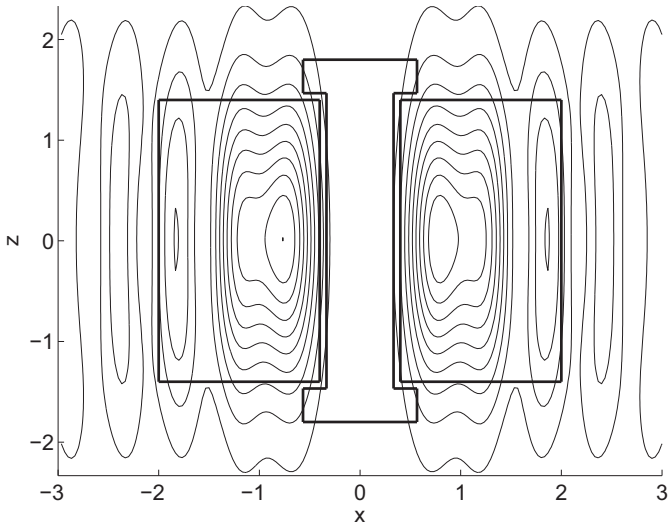

Figure 5. Intensity contour of the LG_{04} incident beam and quatrefoil rotor profile.

We settled for $h = 2.2$ and $r_a = 2.2$ to expedite subsequent calculations. The hub radius r_b was varied, and it can be seen that the torque efficiency drops rapidly for $r_b > 0.4$ (figure 8). In the extreme case, $r_b = r_a$, the rotor becomes a cylinder that is lined up with the beam axis and no torque can be generated.

Still keeping $h = 2.2$ and $r_a = 2.2$, but $r_b = 0$ and varying ϕ, we now look for the optimal blade angle. It appears that the blades should sweep an angle between 35° and 40° (figure 9) to achieve optimal torque.

4. DISCUSSION

The LG_{04} beam produced lower torque efficiency than the LG_{02}. We did not expect that the torque would decrease with increasing l for the LG_{0l} beam since orbital angular momentum per photon is just $l\hbar$. This decrease in torque with increasing l has also been observed by other researchers performing torque measurements with anisotropic spheres;[21] they did not offer a rigorous explanation and one would question the relevance of orbital angular momentum to spinning anisotropic spheres where the spin angular momentum is what we expect to drive the sphere.

One possible explanation is that LG_{04} couples to LG_{00}, in effect shifting the high intensity ring to the centre. On the other hand LG_{02} couples to $LG_{0\ -2}$; the ring remains in the same area but the handedness changes. This suggests the the loss of efficiency of the LG_{04} is due to weak coupling between incident and scattered modes with very little overlap in the plane of the rotor. We propose further investigation by examining the scattering coefficients of the modes in question.

We explored the basic behaviour, namely the torque, of the quatrefoil rotor whilst examining the effects thickness, radius and blade angle by varying only one parameter at a time. This gave us information on the efficiency of the incident beam and approximated a starting point for achieving the optimal dimensions. Further work can be undertaken with a more sophisticated algorithm such as simulated annealing[22,23] whereby the global minimum of the search space (the multi-dimensional space formed by the abovementioned parameters) can be determined.

The symmetry optimization[18] schemes used in conjunction between the DDA and the point-matching methods to formulate the T-matrix have proven to be sufficiently fast; this method is suitable for aiding the design of microrotors and other micromachine components. The reduction of the memory footprint is essential for modelling microrotors as their size would have resulted in interaction matrix RAM requirements that exceed those available on high-end desktop PCs.

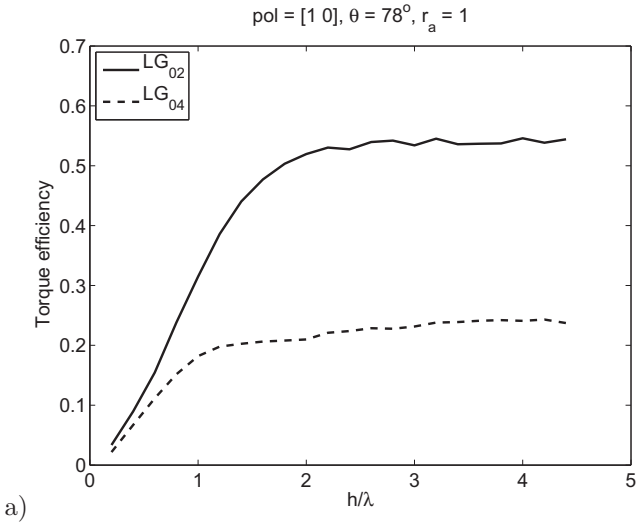

a)

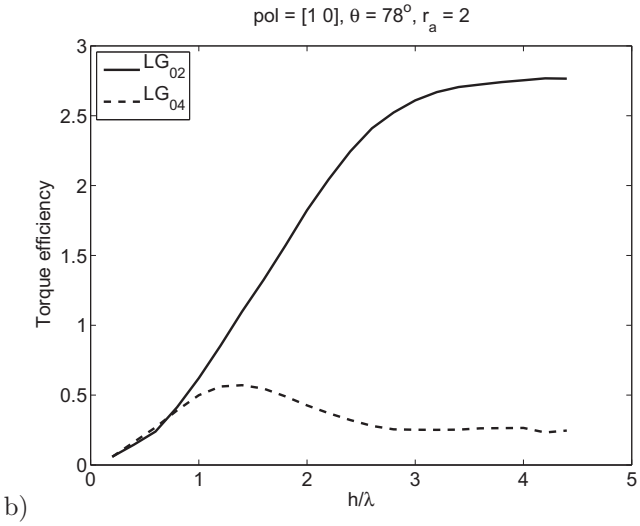

b)

Figure 6. The torque efficiency of the microrotor versus its height at $r_b = 0$ and a) $r_a = 1\lambda$ b) $r_a = 2\lambda$.

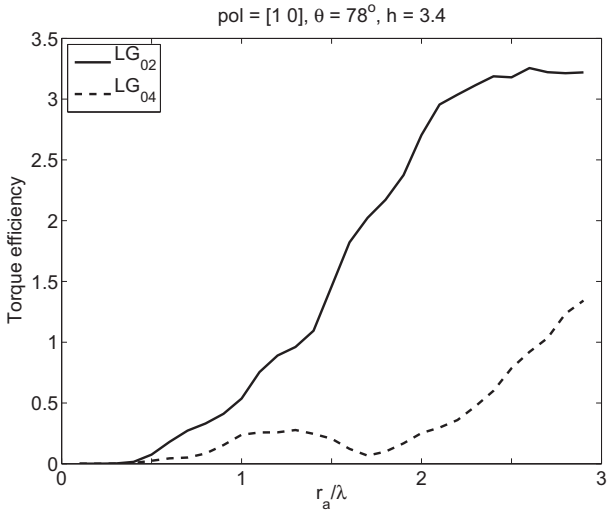

Figure 7. The torque efficiency of the microrotor versus its blade radius at the optimal height of $h = 3.4\lambda$.

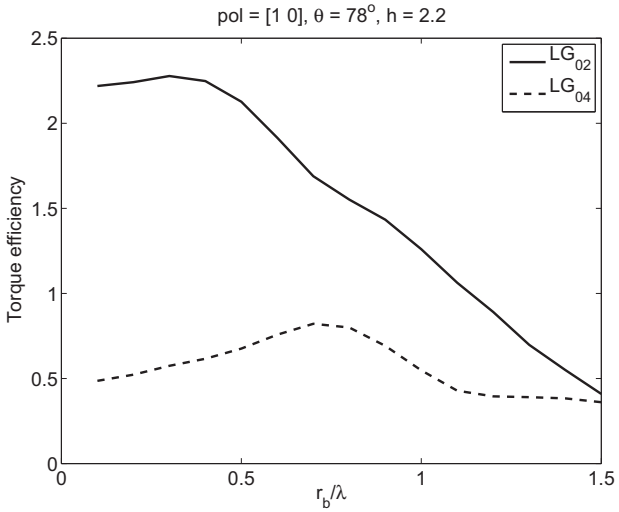

Figure 8. The torque efficiency of the microrotor versus its hub/axle radius at height of $h = 2.2\lambda$ and rotor radius of $r_a = 2.2\lambda$.

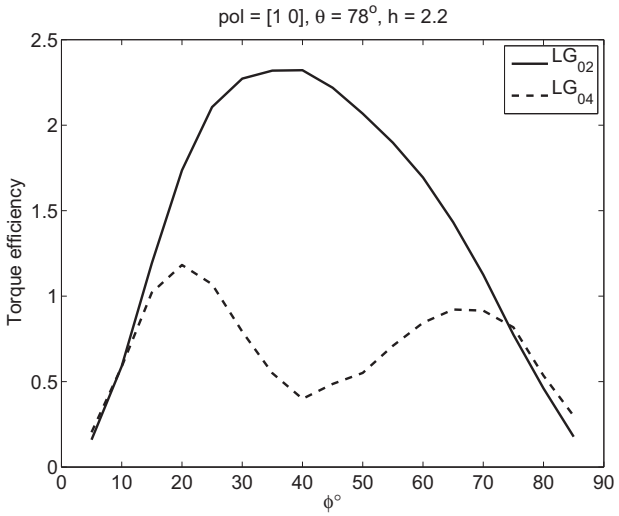

Figure 9. The torque efficiency of the microrotor versus its blade angle at height of $h = 2.2\lambda$ and rotor radius of $r_a = 2.2\lambda$.

REFERENCES

[1] Ashkin, A., Dziedzic, J. M., Bjorkholm, J. E., and Chu, S., "Observation of a single-beam gradient force optical trap for dielectric particles," *Optics Letters* **11**, 288–290 (1986).

[2] Friese, M. E. J., Nieminen, T. A., Heckenberg, N., and Rubinsztein-Dunlop, H., "Optical torque controlled by elliptical polarization.," *Optics Letters* **23**, 1–3 (1998).

[3] He, H., Friese, M. E. J., Heckenberg, N. R., and Rubinsztein-Dunlop, H., "Direct observation of transfer of angular momentum to absorptive particles from a laser beam with a phase singularity," *Physical Review Letters* **75**, 826–829 (1995).

[4] Beth, R. A., "Mechanical detection and measurement of the angular momentum of light," *Physical Review* **50**, 115–125 (1936).

[5] Friese, M. E. J., Nieminen, T. A., Heckenberg, N., and Rubinsztein-Dunlop, H., "Optical alignment and spinning of laser-trapped microscopic particles," *Nature* **394**, 348–350 (1998). Erratum: *Nature* **395**, 621 (1998).

[6] Bishop, A. I., Nieminen, T. A., Heckenberg, N. R., and Rubinsztein-Dunlop, H., "Optical application and measurement of torque on microparticles of isotropic nonabsorbing material," *Physical Review A* **68**, 033802 (2003).

[7] Sato, S., Ishigure, M., and Inaba, H., "Optical trapping and rotational manipulation of microscopic particles and biological cells using higher-order mode Nd:YAG laser beams," *Electronic Letters* **27**(20), 1831–1832 (1991).

[8] Loke, V. L., Asavei, T., Nieminen, T. A., Heckenberg, N. R., and Rubinsztein-Dunlop, H., "Optical microrotors: theory, design and fabrication," *Proceedings of SPIE* **6644** (2007).

[9] Asavei, T., Nieminen, T. A., Heckenberg, N. R., and Rubinsztein-Dunlop, H., "Fabrication of microstructures for optically driven micromachines using two-photon photopolymerization of UV curing resins," *Journal of Optics A* **11**(3), 034001 (7pp) (2009).

[10] Parkin, S. J. W., Knöner, G., Nieminen, T. A., Heckenberg, N. R., and Rubinsztein-Dunlop, H., "Measurement of the total optical angular momentum transfer in optical tweezers," *Optics Express* **14**(15), 6963–6970 (2006).

[11] Nieminen, T. A., Asavei, T., Loke, V. L. Y., Heckenberg, N. R., and Rubinsztein-Dunlop, H., "Symmetry and the generation and measurement of optical torque," *Journal of Quantitative Spectroscopy and Radiative Transfer* **110**, 1472–1482 (2009).

[12] Nieminen, T. A., Loke, V. L. Y., Stilgoe, A. B., Knöner, G., Brańczyk, A. M., Heckenberg, N. R., and Rubinsztein-Dunlop, H., "Optical tweezers computational toolbox," *Journal of Optics A* **9**, S196–S203 (2007).

[13] Mishchenko, M. I., "Light scattering by randomly oriented axially symmetrical particles," *Journal of the Optical Society of America A* **8**(6), 871–882 (1991).

[14] Brock, B., "Using vector spherical harmonics to compute antenna mutual impedance from measured or computed fields," Tech. Rep. SAND2000-2217-Revised, Sandia National Laboratories, Albuquerque, NM (2001). (unpublished).

[15] Purcell, E. and Pennypacker, C., "Scattering and absorption of light by nonspherical dielectric grains," *Astrophysical Journal* **186**, 705–714 (1973).

[16] Draine, B. T. and Flatau, P. J., "Discrete-dipole approximation for scattering calculations," *Journal of the Optical Society of America A* **11**(4), 1491–1499 (1994).

[17] Jackson, J. D., [*Classical electrodynamics*], Wiley, New York (1998). 3rd ed.

[18] Loke, V. L. Y., Nieminen, T. A., Heckenberg, N. R., and Rubinsztein-Dunlop, H., "T-matrix calculation via discrete-dipole approximation, point matching and exploiting symmetry," *Journal of Quantitative Spectroscopy and Radiative Transfer* **110**, 1460–1471 (2009).

[19] Crichton, J. H. and Marston, P. L., "The measurable distinction between the spin and orbital angular momenta of electromagnetic radiation," *Electronic Journal of Differential Equations* **Conf. 04**, 37–50 (2000).

[20] Nieminen, T. A., Heckenberg, N. R., and Rubinsztein-Dunlop, H., "Multipole expansion of strongly focussed laser beams," *Journal of Quantitative Spectroscopy and Radiative Transfer* **79-80**, 1005–1017 (2003).

[21] Simpson, S. and Hanna, S., "Optical angular momentum transfer by Laguerre–Gaussian beams," *Journal of the Optical Society of America A* **26**, 625–638 (2009).

[22] Kirkpatrick, S., Gelatt, C. D., and Vecchi, M. P., "Optimization by simulated annealing," *Science* **220**(4598), 671–680 (1983).

[23] Cerny, V., "Thermodynamical approach to the traveling salesman problem - an efficient simulation algorithm," *Journal Of Optimization Theory And Applications* **45**(1), 41–51 (1985).